International Journal of Engineering Research & Technology (IJERT)
ISSN: 2278-0181
Vol. 9 Issue 02, February-2020

An Approachable Function for Water Flow Obstructed by Pier using Particle Image Velocimetry

Jose Elias Villa Herrera[a], Cornelio Alvarez Herrera[a],
Humberto Silva Hidalgo[a], Jose Luis Herrera Aguilar[a],
Antonio Campa Rodriguez[a]
[a,] Universidad Autónoma de Chihuahua,
Facultad de Ingeniería, Nuevo Campus Universitario,
Circuito Universitario S/N, C.P, Chihuahua,
Chih., México.

Jose Guadalupe Murillo Ramirez[b]
[b,] Centro de Investigación en Materiales Avanzados S. C., Miguel de Cervantes 120,
Complejo Industrial Chihuahua. C.P, México.

***Abstract*:- This research was focused on obtaining a mathematical function, about pier distance / vorticity relationship, of water flow when it is obstructed by a pier at different speeds, using the optical technique called PIV (Particle Image Velocimetry). An hydraulic channel was used, micro spheres of glass seeded in the water as tracking particles of the flow current lines, a 532 nm Lincoln laser lighting equipment, a Phantom M 310 CCD video camera, a cylindrical pier as model, and a processing data software named LaVision DaVis 8 as well as post-processing image software Tecplot-360. In this experimental development, vorticities and abrupt changes of speed and direction near the pier surface were found, which generate scouring. Position about main vorticity, corresponding to the downstream of pier, being plotted. Also, it was visualized that there is a change of direction called downflow in the front part of the pier, reason why this flow was plotted too.**

Keywords: Function; Flow; Scour; Particles; Image; Velocimetry.

1. INTRODUCTION

Land routes are essential parts of communication and performance between communities, transporting assets and people. Bridges are structures that allow us to break the geographic barriers of a road, achieving connectivity from one place to another [7], so, the failure of one of these, implies high costs of repairing [6]. In addition, it generates delays in transportation, loss of accessibility, and in some cases, it could cause human casualties [9]. It is important in the construction of a bridge that crosses a fluvial channel to take into account hydraulic parameters, background materials, foundation geometry, bridge location and maximum flows that can be generated to be able to protect itself from the scour that may occur in that particular section, for its better design [17].

Nowadays it is possible to try to know about the flow of the water when it is obstructed by a cylindrical pier through the technology of images [2], and with this, develop mathematical models that approximate their behavior. Algebraic functions such as those of a variable appear in too many areas of mathematics, in complex analysis, geometry, and numerical theory [16]. The implicit function theorem is one of the most important results for functions of several variables in partial differential equations and numerical analysis [5] Mathematical models have been gaining importance in geometric modeling, visualization, animation and computational graphics for general structured data through curves, surfaces and implicit objects [8].
The goal of this research was to analyze the behavior of the water flow at different speeds, which causes scouring in the bed of a river when it is obstructed by structures such as a cylindrical pier of a bridge, this analysis was performed by using the particle image velocimetry (PIV) optical technique that allowed us to present a new mathematical function obtained from laboratory model measurements.

Scouring is the result of the erosive action of water currents on the bed of the canal, especially in rainfall seasons and the floods caused by rivers [15;17]. The scouring in a structure, in general terms, occurs due to the flow that, when obstructed, divides, goes down, striking the bottom and subsequently surrounding the structure geometry, causing vortices by the turbulent flow [13]. The scouring mechanism is associated with three-dimensional flow separation on the face upstream of the obstruction structure and a periodic vortex at the foot of it [3]. Due to the obstruction, a strong gradient of pressure is generated which causes the separation of the flow generating a kind of vortex called the horseshoe, being the main cause of the scouring [14], which have a behavior similar to that of a vacuum cleaner weakening downstream by accumulating sediments [12]. In Figure 1 it is shown the behavior of water flow interacting with a cylindrical pier.

International Journal of Engineering Research & Technology (IJERT)
ISSN: 2278-0181
Vol. 9 Issue 02, February-2020

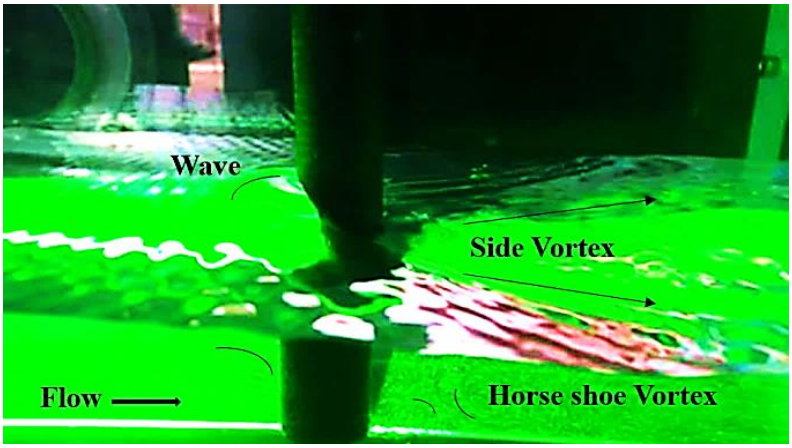

Figure 1. Behavior of water flow interacting whit a cylindrical pier [2;12].

There are some technologies for fluid mechanics analysis and PIV is one of them. Particle Image Velocimetry is a non-destructive real time technique, which has been the basis of and very useful for experimentation with fluid movements and behavior, being able to obtain vectors and their vorticity. For the field of hydrodynamics and dynamics, the study of the speed and direction measurements of a flow are important aspects for its comprehension. [11].

PIV is known to be an optical procedure for the observation of fluids, carried out in different fields of interest. The speed rate is obtained by capturing particles inside the flow by consecutive taken images, which are in two dimensions. [4].

PIV uses as principle to measure the distance, Δs, particles inside a flow in movement during a very short time period Δt. The U speeds calculated under the following equation:

$$U = \frac{\Delta s}{\Delta t} \qquad (1)$$

The particles are suspended within the flow and with the same speed, which are illuminated by laser lighting equipment, so that they can be captured by the camera. The position of the particles for each pulse of light is recorded and must be at least two pulses Δs which is the path of the two captures through the camera [4]. In Figure 2 is shown example of images movement 2(a), 2(b) and 2(c) used in PIV.

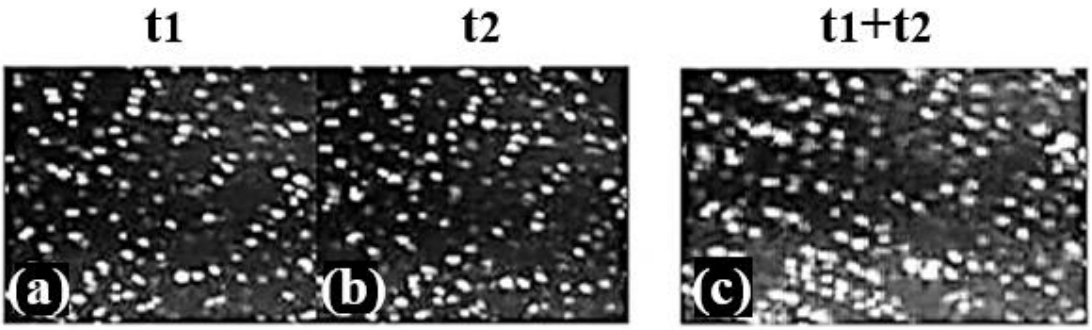

Figure 2. Example of images movement 2(a), 2(b) and 2(c) used in PIV [1;10].

Figures 2(a) and 2(b), represent two consecutive images. Then, these types of images are processed to obtain the single individual movement figured by the particles between one image and the other.

Figure 2 (c) represent a super position movement of each one of these particles which can be observe as a pair of particles going from time t1 to time t2, the crossed correlation is used to locate the most similar position between two images such as is presented [1].

For the testing with crossed correlation, PIV images are separated into little frames areas called “interrogation zones”. An interrogation zone is an area of an image *f*, that is mean to say sub-image of *f*. It is supposed that all the particles that are into an interrogation zone, move in an evenly movement. The standard algorithm of PIV is about of processing two interrogation zones of the same magnitude and with the same coordinates within the image. One zone is from the first image and the other from the second image as shown in Figure 3 [1]. The interrogation zones must be processed in order to find an average of movement of particles in the two images. In this way the methodology consists in calculating directly the crossed correlation between the two zones:

International Journal of Engineering Research & Technology (IJERT)
ISSN: 2278-0181
Vol. 9 Issue 02, February-2020

$$f(x,y) \bullet g(x,y) = \sum_{i=-M}^{M} \sum_{j=N}^{N} f(i,j)g(i+x,j+y) \quad \textbf{(2)}$$

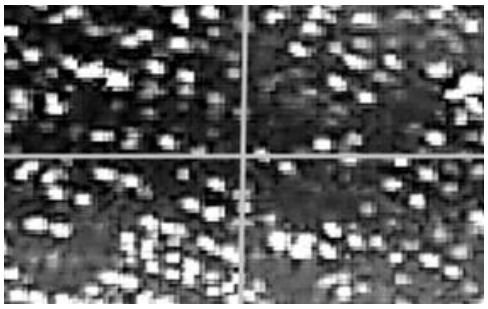

Figure 3. PIV Images separated in interrogation zones [1;10]

For x= 0, ±1, ±2 … . . − 1; 0, ±1, ±2 … . . − 1, where *f(x, y)* is the sub-image agrees to the first interrogation zone, *g(x ,y)* is the sub-image associate to the second zone, and *M* and *N* are the width and the height in pixels of the interrogation zone, one by one. The process is about of moving a sub-image over the other and aggregates the products of the estimation where overlapping occurs. Each estimation is saved as a matrix called "matrix or plane of crossed correlation", in the position that constitutes the moving of the second sub-image over the first one.

2. METHODS

It was used a rectangular water channel with 0.50 m long, 0.15 m deep and 0.15 m width, with a 1.5HP electric pump. The walls of the channel are of transparent acrylic, in order to let the 532 nm Lincoln laser light, go through the micro 9-13μm spheres of glass planted in the water. A water container with a capacity of 200 liters. An ABS plastic made cylindrical pier of 2 cm diameter and 15 cm long was used to simulate the effect of the obstruction. A Phantom M 310 CCD video camera and a processing image software named LaVision DaVis 8 were used to get general data, likewise Tecplot 360. In Figure 4 it is shown equipment used.

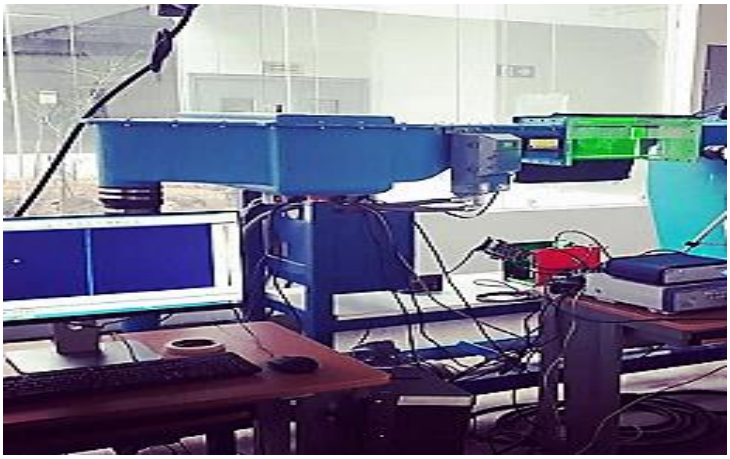

Figure 4. Equipment used to develop the experiment.

The experiment was carried out in a darkened area with the purpose of recording the dynamics of particles and water flow by means of the PIV optical setup. A longitudinal slope of zero percent was applied to the water flow in the channel. The experiment was done in accordance to the Reynolds number, from laminar to turbulence flow with flow rates of 0.107, 0.44, 0.77, 1.066, 1.58 L/s for upstream flow of pier, then 1.58, 2.22, 2.72, 3.24, 3.26 L/s for downstream flow. Potable water without any special treatment was used, reaching a level of water equal to 9.0 cm. In Figure 5 it is shown pier crossed by laser lighting.

International Journal of Engineering Research & Technology (IJERT)
ISSN: 2278-0181
Vol. 9 Issue 02, February-2020

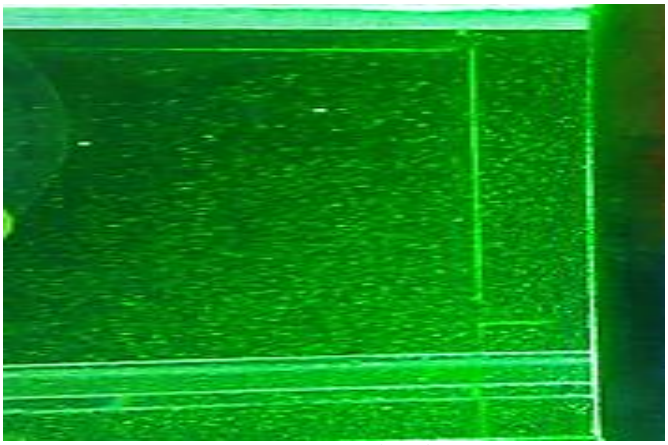

Figure 5. Pier crossed by laser lighting front flow with glass spheres.

A green light sheet emitted by the laser equipment crossed parallel to the cylindrical pier along the water channel, illuminating the trace of the glass spheres with more than 25 of them per frame, synchronized by a controller appliance to the CCD camera leveled, focused and scaled dimensionally to the object that was at 50cm long, it took 40 images of 24 x 24 pixels with a capture time between them equivalent to 700μs. In this way the movement of the spheres can be seen in detail, with the vorticity and the vectors in the water flow in the front and back, due to the obstruction generated by the model, especially the high-speed ones. It was verified that the speed of the water channel was very close to the speed of the digital images flow vectors obtained by the camera using LaVision Davis 8 software. In figure 6,7 and 8 it is shown parts of equipment used.

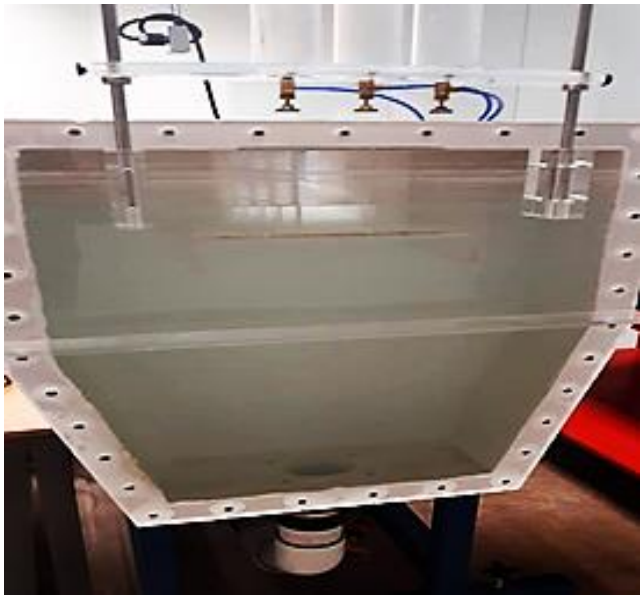

Figure 6. Water container – 200lts capacity.

Figure 7. Water channel and pier model inside.

International Journal of Engineering Research & Technology (IJERT)
ISSN: 2278-0181
Vol. 9 Issue 02, February-2020

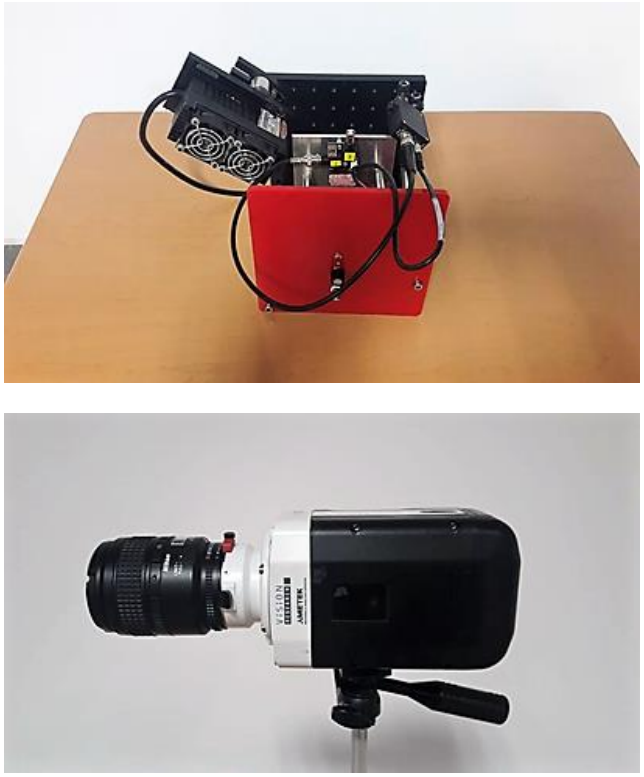

Figure 8. The 532 nm Lincoln laser light and Phantom M 310 CCD video camera.

The image processing software LaVision DaVis 8 greatly facilitated the task to obtain the resolution of the images, specific areas to observe quantity and size of the vectors, as well as the division of colors of the vorticity, among other aspects. In Figure 10 it is shown the schema of working process.

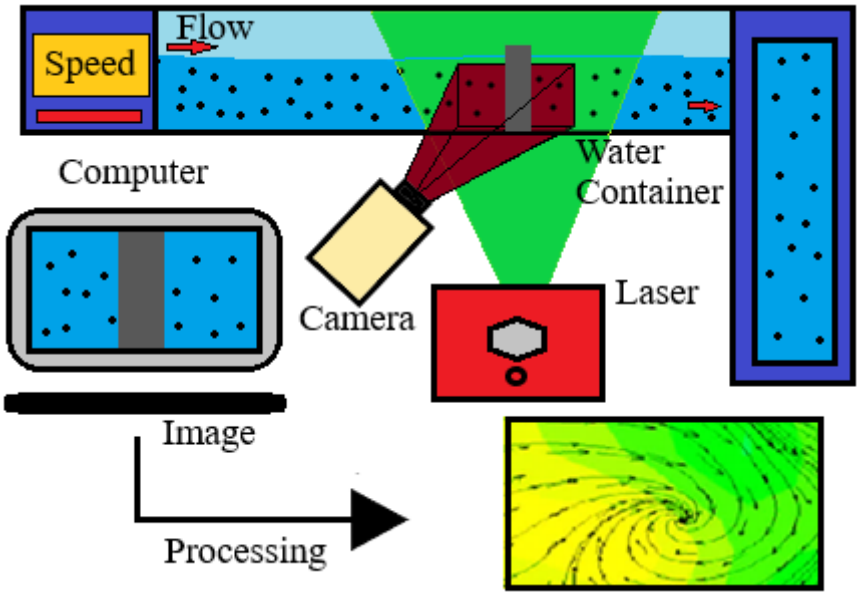

Figure 9. Schema of working process.

3. RESULTS

The study areas in the front and the back next to the cylindrical pier are shown below, which were enabled by the octave software and subsequently processed at different speed. Figure 11. shows the study areas.

International Journal of Engineering Research & Technology (IJERT)
ISSN: 2278-0181
Vol. 9 Issue 02, February-2020

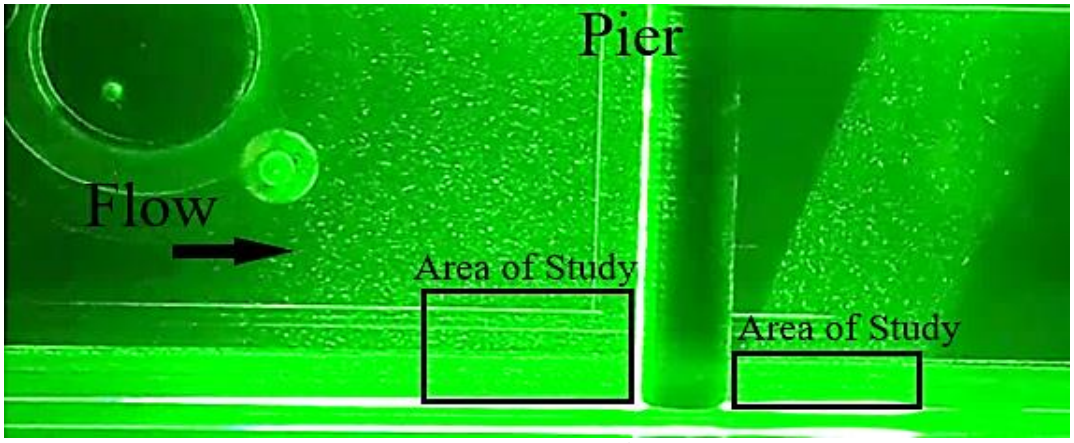

Figure 10. Selected areas of study.

In Figures from 11 to 15 show vorticity at different flow rates, corresponding to the upstream, frontal study area. The flow of water at low flow rate is returned when it hits the pier, which is known as retro flow, in addition to a tendency to go to the bottom, as the flow rate increases this tends to go linearly over the pier strongly. In Figure 21ti is shown a developed function about radius size generated by retro flow at different speeds. The measurements for radius size were taken from same upstreamfigures by visualization. Also were obtained standar deviation (S) and correlation (R-Sq).

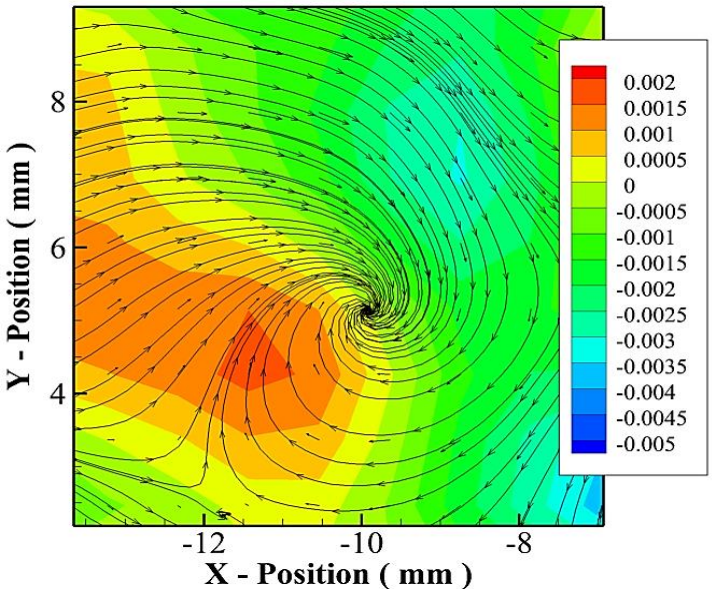

Figure 11. Flow Rate 0.107 L/s: Very low laminar flow, it is revealed the circumference or also called retro flow, because of the obstruction of pier.

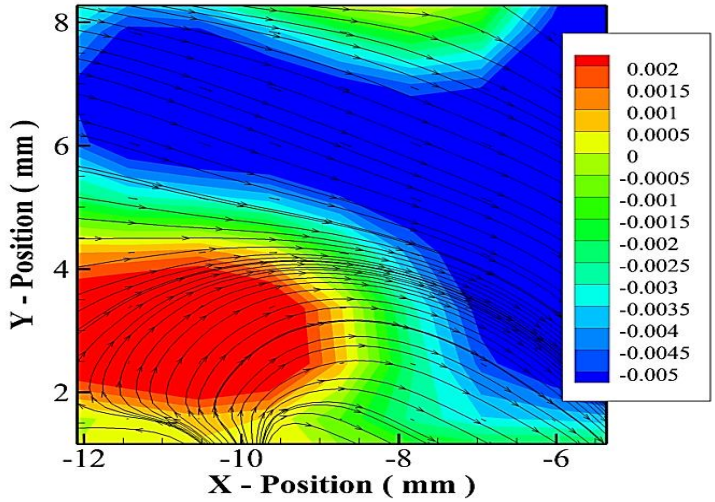

Figure 12. Flow Rate 0.44 L/s: Circular line begins bending with a straight angle trend, retro flow has diminished a little, because water flow is stronger and start surpassing pier by sides.

International Journal of Engineering Research & Technology (IJERT)
ISSN: 2278-0181
Vol. 9 Issue 02, February-2020

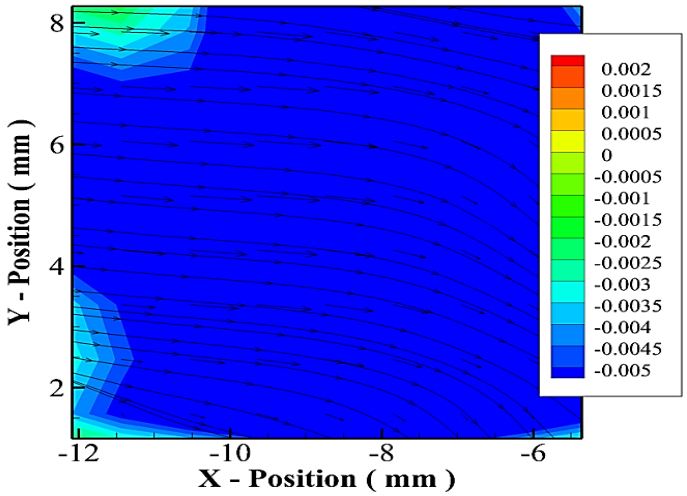

Figure 13. Flow Rates 0.77 L/s: Water flow is getting a straight linear trend due to the speed increase. Also a it is shown a stronger downflow going to the bottom.

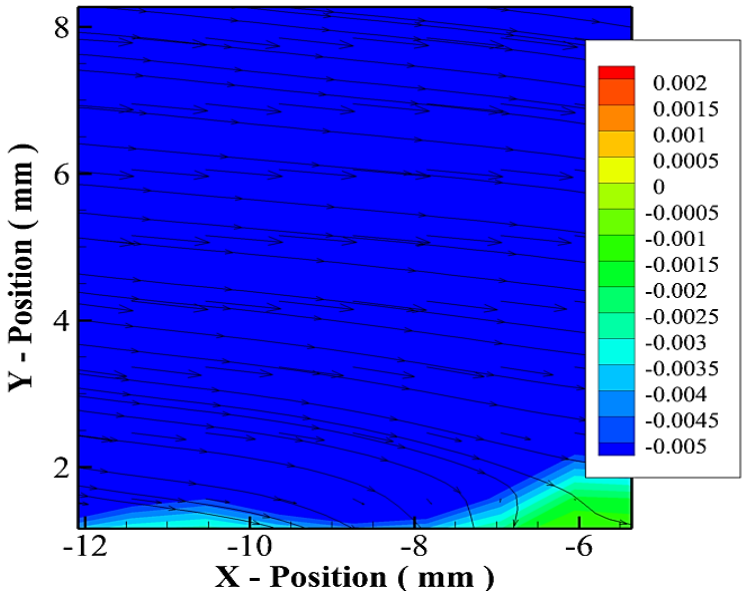

Figure 14. Flow Rates 1.066 L/s: Almost linear water flow, the entire vortex can be seen in the bottom.

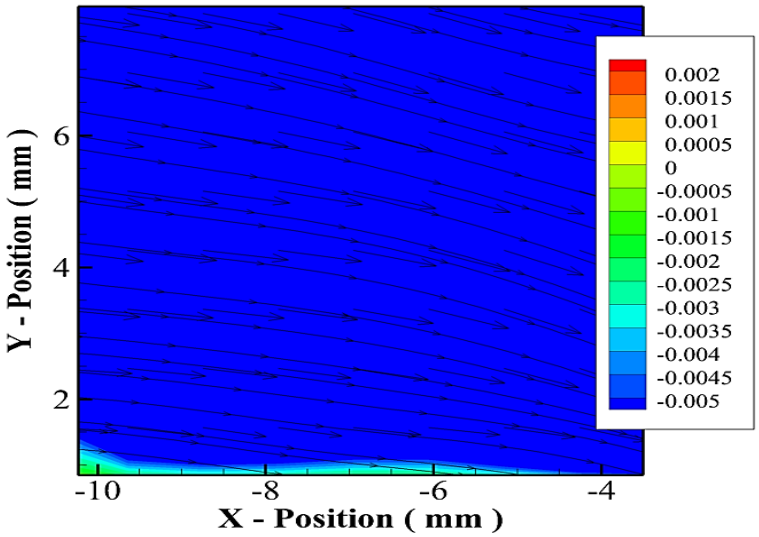

Figure 15. Flow Rates 1.58 L/s: Total linear water flow, the entire vortex can be seen in the bottom touching the pier. Most of water flow surpass pier by sides.

International Journal of Engineering Research & Technology (IJERT)
ISSN: 2278-0181
Vol. 9 Issue 02, February-2020

In Figures from 16 to 20 show vorticity at different flow rates corresponding to the downstream, rear study area. At low flow rate the turbulence is minimal, but as it increases high vorticity is generated and a water flow hits the pier strongly. In Figure 22 it is shown a developed function about distance between pier and vortex at different speeds. The measurements for distance were taken from same downstream figures by visualization. Also were obtained standar deviation (S) and correlation (R-Sq).

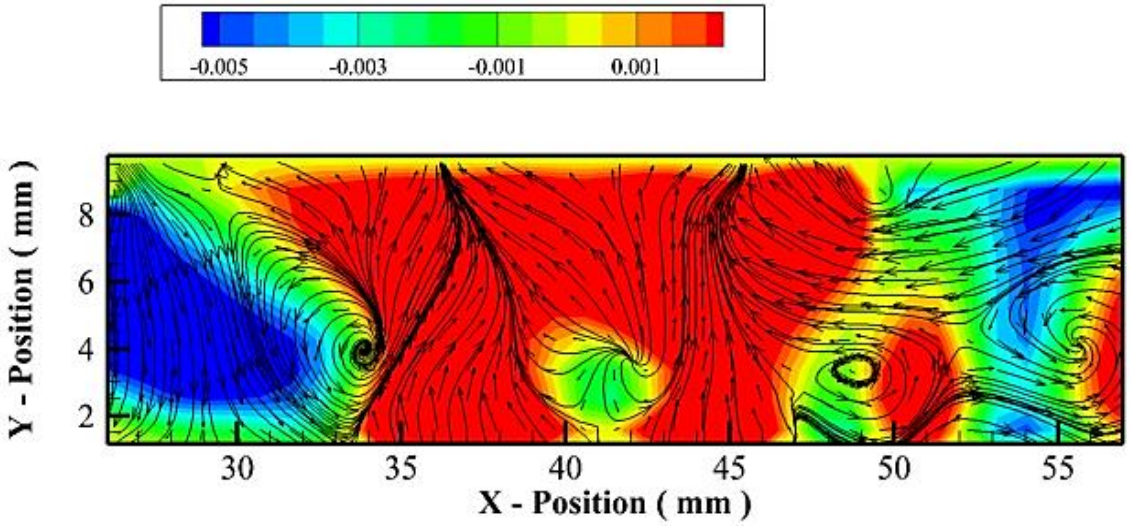

Figure 16. Flow Rate 1.58 L/s: It is no seen strong vortex next to the pier.

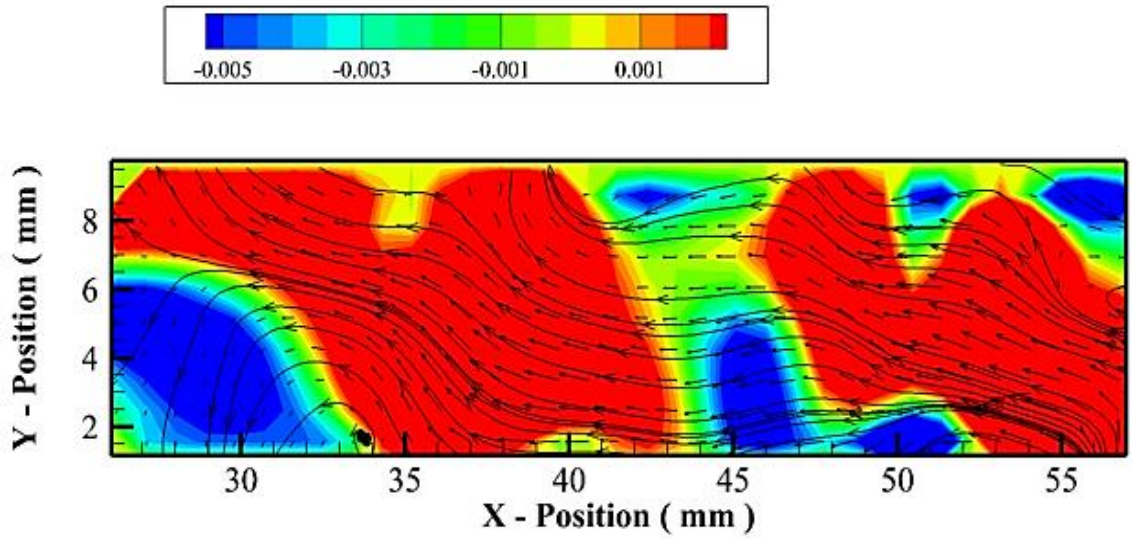

Figure 17. Flow Rate 2.22 L/s: Vortex and vectors are totally against the pier.

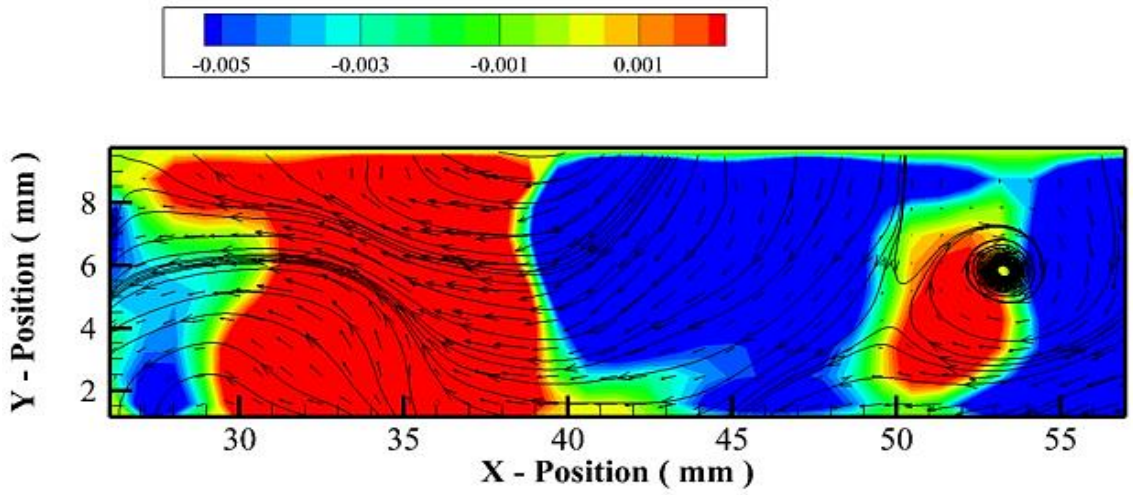

Figure 18. Flow Rate 2.72 L/s: It is shown vortex and vectors now are almost together the pier.

International Journal of Engineering Research & Technology (IJERT)
ISSN: 2278-0181
Vol. 9 Issue 02, February-2020

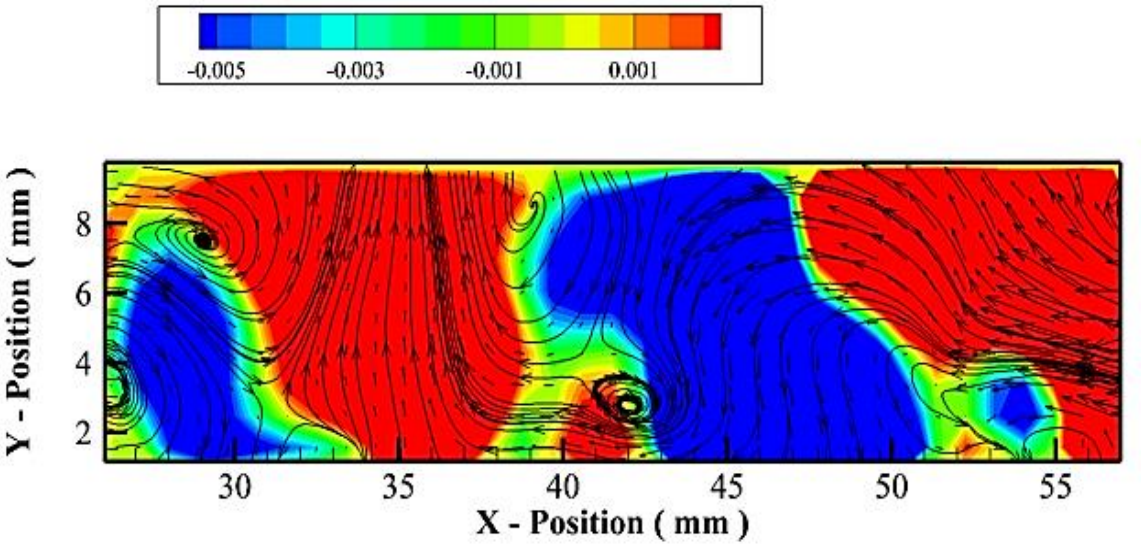

Figure 19. Flow Rate 3.24 L/s: Now it is shown vortex and vectors are together the pier.

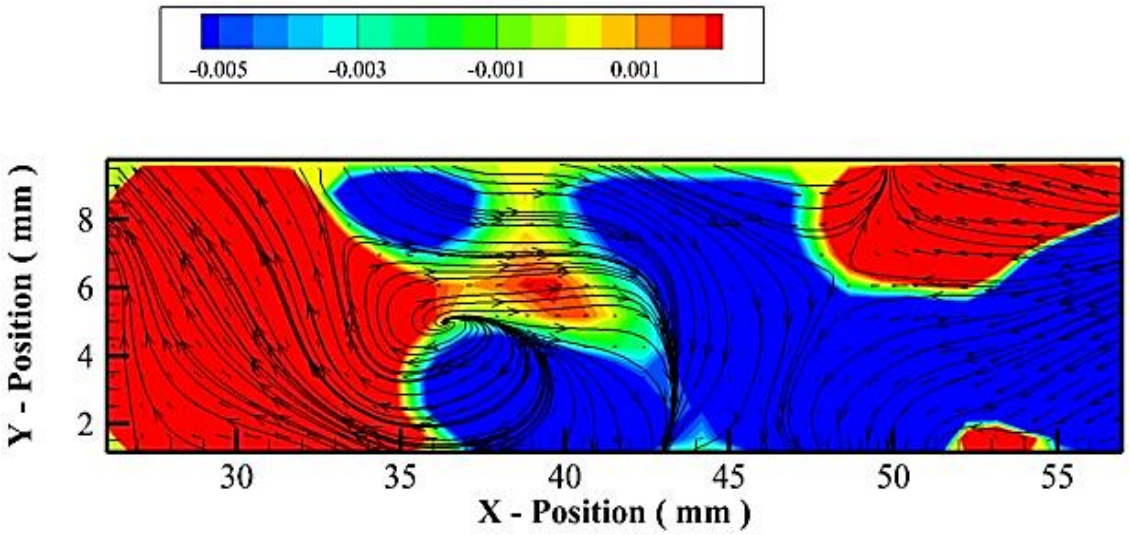

Figure 20. Flow Rate 3.26 L/s: It is appreciated vortex and total vectors together and hitting strong against the pier.

In Figure 21 and 22 it is shown an example of how the values were obtained by visualization respectively, for the radius according to the circumference that belongs to the downflow, and the distance between the vortex and pier until vectors hitting it, for the downstream.

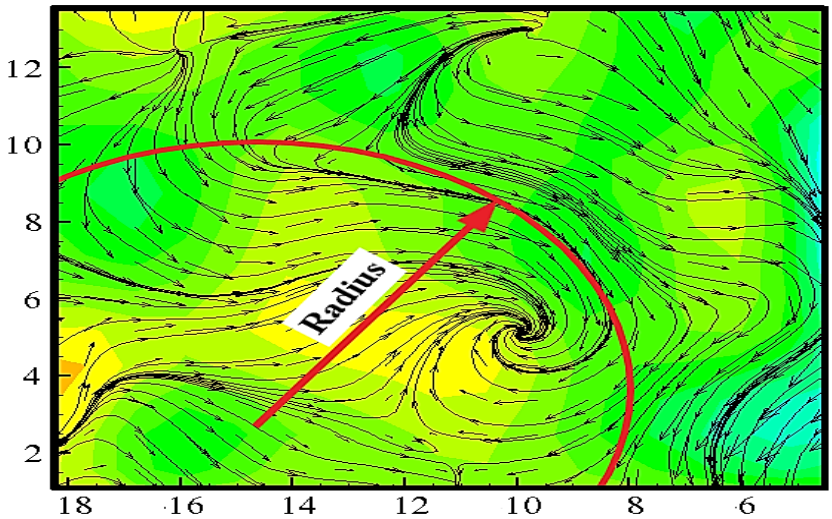

Figure 21. Measurements for radius size, corresponding to the upstream, front study area.

International Journal of Engineering Research & Technology (IJERT)
ISSN: 2278-0181
Vol. 9 Issue 02, February-2020

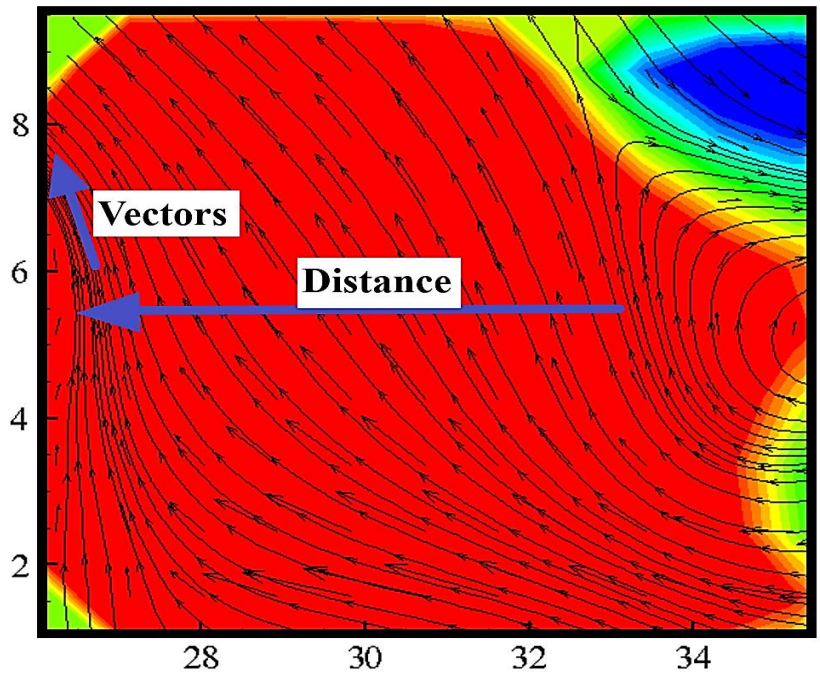

Figure 22. Measurements for distance, corresponding to the downstream, rear study area.

3.1. Mathematical Relations Front Side

Table 1 shows the data corresponding to flow rate, radius (obtained by visualization of the figures 11 to 15) of curvature of the vortex and tendency of the flow belonging to the front side area.

Flow Rate (L/s)	Radius (mm)	Flow form trend
0.107253	7	Low
0.44794	4	Medium
0.7760094	2	Moderated High
1.066224	0.5	High
1.583564	0.0	Pretty high

Table 1. Flow Rate, radius and flow trend.

In table 2 shows the scale magnitude, corresponding to Reynolds number for hydraulic channel ($500 \leqslant Re \leqslant 2000$) front side. $Re = \rho v R/\mu$, where: $\boldsymbol{\rho}$ = water density; $\boldsymbol{v}$ = water speed; $\boldsymbol{R}$ =hydraulic radius and μ =water dynamic viscosity.

Flow Rate L/s	Speed (m/s)	Reynolds (Re)
0.107253	0.0084	235.87
0.44794	0.033	930.41
0.7760094	0.0574	2164.84
1.066224	0.0803	2253.96
1.583564	0.1173	3289.21

Table 2. Reynolds number.

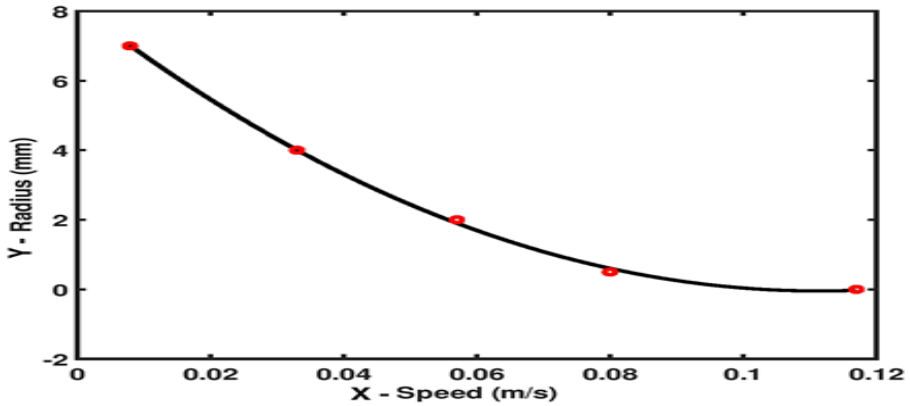

Figure 23. Function is observed by the black line, corresponding to the upstream, front study area.

International Journal of Engineering Research & Technology (IJERT)
ISSN: 2278-0181
Vol. 9 Issue 02, February-2020

The points X and Y corresponding to the experiment are plotted in red circles and the adjusted function is observed by the black line, with a confidence level of 95%, using the fitted line application of the Octave software, generating a grade 2 equation due to it being the closest one when crossing the points. Fitted line plot: Y = 8.199 – 148.1 X + 665.4 X^2; S = 0.107394; R-Sq= 99.90%.

$$Y = f_1X^2 + f_2X + f_3 \quad \textbf{(3)}$$

3.2. Mathematical Relations Rear Side

Table 3 shows the data corresponding to Flow Rate, distance (obtained by visualization of the figures 16 to 20) to pier and tendency of the flow belonging to the front side.

Flow Rate L/s	Distance between Pier and Vortex (mm)	Flow form trend
1.583564	3.5	Low
2.220775	3.0	Medium
2.725496	2.1	Moderated High
3.242836	1.0	High
3.268072	0.8	Pretty high

Table 3. Flow Rate, pier distance and flow trend.

In table 4 shows the scale magnitude, corresponding to Reynolds number for hydraulic channel (500⩽Re⩽2000) rear side $Re = \boldsymbol{\rho v R}/\mu$.

Flow Rate L/s	Speed (m/s)	Reynolds (Re)
1.583564	0.1173	3289.21
2.220775	0.16309	4373.44
2.725496	0.2018	5661.11
3.242836	0.2472	6932.24
3.268072	0.25002	7010.87

Table 4. Reynolds number.

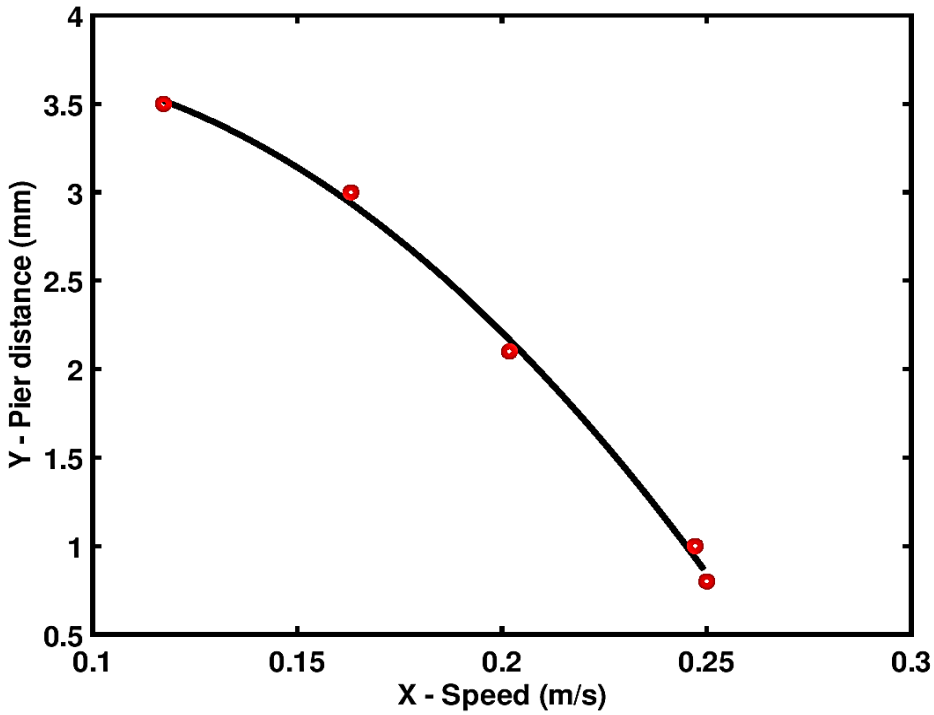

Figure 24. Function is observed by the black line, corresponding to the downstream, rear study area.

Same way the points *X* and *Y* corresponding to the experiment are plotted in red circles and the adjusted function is observed by the black line, with a confidence level of 95%, using the fitted line application of the Octave software, generating a grade 2 equation due to it being the closest one when crossing the points. Fitted line plot: Y = 3.357 + 11.47 X – 86.06 X^2; S =0.0867; R–Sq = 99.7%.

$$Y = f_1X^2 + f_2X + f_3 \quad \textbf{(3)}$$

International Journal of Engineering Research & Technology (IJERT)
ISSN: 2278-0181
Vol. 9 Issue 02, February-2020

4. CONCLUSIONS

Two lateral areas were selected, one upstream on the frontal side and another one downstream on the rear side, next to the cylindrical pier, in such a way that was possible to appreciate the behavior of the water flow, responsible of scour. In Figure 10 it is shown the selected areas. Work began at very low speed where the water flow went from very low to very high, where the water flow becomes abrupt and turbulent causing the scour. It was observed that the flow of the water in the selected frontal part, at low speed creates a circumference, generating a retro flow because the obstruction. As the speed increases, this circumference and the retro flow are lost, acquiring a linear form. Regarding the rear side, at low speed no turbulence was observed, but as the speed increases, the turbulence reached the pier. Upstream, as shown by the software's imagery, the formation of a vortex was clear due to a retro flow generated by the obstruction of the pier, where at the same time the water hits the bottom, known as down flow and on the other hand passes around, this vortex decreased as the flow force increased, with a tendency to be more linear as shown by the radius / speed function. Downstream regarding side and horse shoe vortex, they are moderate and away from the pier when the flow force is low but when it increases, it is quickly the opposite where the formation of large vortices can be seen hitting the bottom and pier, as shows by pier distance / speed function.

Particle Image Velocimetry (PIV) optical technique was suitable to develop this job in a lab controlled situation. It was able to watch the water flow behavior, understanding how this, rises the bottom soil in a river or water channel due to obstruction like a cylindrical pier.

A quadratic function was selected for both areas of study, due to it being the closest fit with better points obtained from parameters pier distance, radius and speed. With a mathematical function, estimating water channel highest speed, we could obtain the critical theoretical vortex distance to the pier in terms of a risk of scour, as a part as a measure of protection.

Further work must be made, related to function improvements, such different geometric piers, different pier thickness and scour at abutments.

6. REFERENCES

[1] Adrian, Ronald J. “Particle-Imaging Techniques for Experimental Fluid Mechanics.” *Annual Review of Fluid Mechanics*, vol. 23, no. 1, 1991, pp. 261–304.

[2] Campa, Antonio, Fernando R., Astorga, Cornelio Alvarez, Jose G., Murillo and. Guadalupe Estrada. “Enhanced Method of Particle Image Velocimetry Applied To Measure the Scour Phenomena in Bridge Piers.” *International Journal of Civil Engineering (IJCE)* , vol. 5, no. 1, 2016, pp. 69–82.

[3] Bijan, Dargahi. “Controlling Mechanism of Local Scouring.” *Journal of Hydraulic Engineering*, vol. 116, no. 10, American Society of Civil Engineers, Oct. 1990, pp. 1197–214, doi:10.1061/(ASCE)0733-9429(1990)116:10(1197).

[4] Çengel, Yunus A., and John M. Cimbala. “*Fluid Mechanics.*” *Fundamentals and Applications Third Edition in SI Units Chapter 15 INTRODUCTION TO COMPUTATIONAL FLUID DYNAMICS*. 2014, pp. 1–27.

[5] Dontchev, Asen L., and R. Tyrrell Rockafellar. “*Implicit Functions and Solution Mappings.* .” *A View from Variational Analysis* . 2nd 2014, Springer New York , 2014, doi:10.1007/978-1-4939-1037-3.

[6] Fisher, Murray, et al. “A Novel Vibration-Based Monitoring Technique for Bridge Pier and Abutment Scour .” *Structural Health Monitoring* , vol. 12, no. 2, SAGE Publications , 2013, pp. 114–25, doi:10.1177/1475921713476332.

[7] García Giraldo, John Mario, et al. “Bridge Infrastructure in Secondary Roads of Antioquia.” *Revista EIA*, vol. 11, no. 22, 2015, pp. 119–31, doi:10.14508/reia.2014.11.22.119-131.

[8] Gomes, Abel J. P. . “*Implicit Curves and Surfaces.*” *Mathematics, Data Structures and Algorithms* . Springer London , (2009), doi:10.1007/978-1-84882-406-5; 9781848824058.

[9] Li, Hua, et al. “Parallel Walls as an Abutment Scour Countermeasure .” *Journal of Hydraulic Engineering* , vol. 132, no. 5, American Society of Civil Engineers , (2006), pp. 510–20, doi:10.1061/(ASCE)0733-9429(2006)132:5(510).

[10] Lopez Hinojoza, Marisol. “*Un Nuevo Algoritmo En La Técnica d|e Velocimetría Por Imágenes de Partículas*”. (2006), pp. 1–137, https://148.204.65.177/sitioCIC/images/sources/cic/tesis/B031210.pdf.

[11] Martinez-Ramírez, J. D., and Fj Gonzalez. “Velocímetro de Particulas Basado En Imagenes Digitales.” *Cenam.Mx*, (2015), pp. 1–5, https://www.cenam.mx/memsimp06/Trabajos Aceptados para CD/Posters/P-15.pdf.

[12] Melville, B. W. “Local Scour at Bridge Abutments.” *Journal of Hydraulic Engineering*, vol. 118, no. 4, (1992), pp. 615–31, doi:10.1061/(ASCE)0733-9429(1992)118:4(615).

[13] Moncada M., Alix T., et al. “*Experimental Study about Scour Protection at Circular Piers; Estudio Experimental Sobre Protección Contra La Socavación En Pilas Circulares*.” *Revista Tecnica* , vol. 30, no. 2, Universidad del Zulia - Facultad de Ingenieria , (2007), p. 157.

[14] Raudkivi, Arved J. “Functional Trends of Scour at Bridge Piers.” *Journal of Hydraulic Engineering*, vol. 112, no. 1, (1986), pp. 1–13, doi:10.1061/(ASCE)0733-9429(1986)112:1(1).

[15] Santiago, Maria, E. “Hidráulica de ríos. Socavación en ríos, puentes y carreteras. ” Instituto Politectico Nacional. Escuela de Ingeniería y Arquitectura.

[16] Wallach, Nolan, and Gabriel Daniel Villa Salvador. “*Topics in the Theory of Algebraic Function Fields*.” Birkhäuser Boston , (2006), doi:10.1007/0-8176-4515-2.

[17] Yang, Han-Chung, and Chih-Chiang Su. “Real-time River Bed Scour Monitoring and Synchronous Maximum Depth Data Collected during Typhoon Soulik in 2013 .” *Hydrological Processes* , vol. 29, no. 6, Wiley Subscription Services, Inc , (2015) , pp. 1056–68, doi:10.1002/hyp.10219.